Tris(Keto-Hydrazone): A fully integrated highly stable and exceptionally sensitive H_2S capacitive sensor

Saravanan Yuvaraja[1‡], Veerabhadraswamy N. Bhyranalyar[2‡], Sachin A. Bhat[2], Mani Teja Vijjapu[1], Sandeep G. Surya[1], C. V. Yelamaggad[2]*, and Khaled Nabil Salama[1]**

[1]Saravanan Yuvaraja, Dr. Sandeep G. Surya, V. Mani Teja and Prof. Khaled N. Salama
Sensors Lab, Advanced Membranes and Porous Materials Center,
Computer, Electrical and Mathematical Science and Engineering Division,
King Abdullah University of Science and Technology (KAUST),
Thuwal, 23955-6900, Kingdom of Saudi Arabia

[2] Dr. Veerabhadraswamy N. Bhyranalyar, Dr. Sachin A. Bhat, Prof. C. V. Yelamaggad
Centre for Nano and Soft Matter Sciences (CeNS),
Jalahalli, Bengaluru 560 013, India.

Keywords: Hydrazones, Nanostructures, H_2S sensor, thin-films, porous polymer

Here a novel tris(keto-hydrazone) monomer having secondary amines and alkoxy groups to detect toxic H_2S gas is reported. The as-synthesized tris(keto-hydrazone) monomer is successfully integrated on a micro-fabricated device to realize an organic capacitive sensor. The organic sensor's quantitative detection capability towards H_2S gas and it's specificity against the other toxic gases and volatile organic compounds (VOCs) is investigated. The capacitance sensor achieved an excellent sensitivity (80% ppm^{-1}) toward H_2S gas with an experimental limit of detection of around 25 ppb. Besides, the fabricated capacitive sensor displayed minimal response to humidity (0.005% RH^{-1}), and high ambient stability (~8 months) without compromising sensing performance. Furthermore, the EDX spectrum analysis confirmed the adsorption of sulfur atoms over the surface of the monomer after the exposure to H_2S gas. After that, a short purge of N_2 gas would suffice to revive the whole device and can work with negligible losses.

1. Introduction

In recent years, there has been an exponential surge in air pollution due to the extensive establishment of chemical-intensive pharmaceutical and oil-based industries.[1] [2] Toxic

emissions are one of the grave concerns since it has taken a heavy toll on human well-being and the environment.[3] [4] For instance, hydrogen sulfide (H_2S) is a well-known hazardous gas that inhibits chemical asphyxiation behavior.[5], [6] According to the Occupational Safety and Health Administration (OSHA) guidelines, human beings are prone to severe respiratory problems when exposed to H_2S concentration between 2 and 5 ppm.[7] [8] [9] Catalytic gas sensor technology, invented in 1926, is recorded to be the first modern age gas detection system that possesses significant advantages, including affordable, insensitive to humidity and appreciable reproducibility.[10] [11] [12] Alongside, the system has certain drawbacks like poor sensing performance and the employed solid-state catalyst are highly poisonous that has the potential to cause severe health concerns when it comes in contact with the users.[10, 13] This was followed by electrochemical gas sensors that are commercially available to sense a wide range of gases.[14] [10, 15] [16] This technology has gained increased attention in a short period due to easy tunability of diffusion barriers on the surface of the porous membrane,[17] but poor chemical stability drastically declines its long-term durability.[18] Similarly, metal oxide semiconductor (MOS) sensors achieve high sensing performance only when operated at elevated temperatures that, in turn, requires more operating power.[19] [20] [21] Given this, it is vital to develop room-temperature operating, low cost and compact gas sensors with excellent sensing performance and ambient stability. [22] [23]

Porous organic materials have been used in multiple applications to date.[22] [24] One of the porous and multifaceted functional group in chemistry are hydrazones; these systems can be found in various chemical structures which are being used for a plethora of different technological applications. The diverse behavior of hydrazone arises due to the presence of azomethine (C=N-N) group, which makes it useful in various fields.[25] A close study of hydrazone structure has revealed that the hydrazone functional group possesses some of the unusual properties such as an exhibition of both electrophilic as well as nucleophilic behaviour,

the existence of acidic proton on the nitrogen, conformational isomerism at C=N bond, etc.[26],[27]

One crucial member of this hydrazone family is tris(keto-hydrazone), a tautomeric structure, first realized by Lee et al.,[28] in the early 2000s. These systems, due to their dynamic architecture, are uniquely placed in the hydrazone family. Literature studies have revealed that these systems are capable of undergoing keto-hydrazone tautomerism readily. Due to the presence of their extensive cage-like structures coupled with the electronic properties such as acidity, nucleophilicity, etc. they are highly sought after candidates for different sensing applications.[29],[30] They are being used as molecular switches and sensors for the detection of various ions and small organic molecules.[25],[31]

Herein, for the first time, we have successfully integrated the secondary amine groups into the hydrazone framework to realize tris(keto-hydrazone) monomer organic thin-film as a novel H_2S gas receptor layer. As is well-known tris(keto-hydrazones) are a unique member of the hydrazone family. Their higher pore density and specific functional groups in 3D structure allow them to pass different gases through and concomitantly identify specific analytes (H_2S). Concurrently, the surface potential of these hydrazones are relatively high and can play a crucial role in leveraging the interaction with analytes. Their photophysical behavior is vital given the thought that they can be incorporated in devices as charge-carrier transport layers. Using the CMOS compatible fabrication approach, we have realized the interdigitated electrode (IDE) sensor on the robust Si/SiO_2 substrate wherein we have drop-casted our organic material to test its sensing capabilities toward H_2S gas. Thereafter, the morphology, surface charge distribution, optical characteristics, and gas-binding properties of organic material are explored using Field emission scanning electron microscopy (FESEM), Kelvin probe force microscopy (KPFM), UV-Vis-NIR spectroscopy and Energy-dispersive X-ray spectroscopy (EDX) characterizations respectively. Our tris(keto-hydrazone) chemi-capacitive sensor have shown exceptional sensitivity and specificity toward target H_2S gas, having 25 ppb as an experimental limit of

detection (LOD). Moreover, the ambient conditions and humidity had a minimal impact on the sensing performance of our sensor.

2. Results and Discussion

Capacitance based sensing is a widely accepted transduction process owing to its temperature stability and minimal complexity.[32] Earlier, Omar et al. [33] have proposed a highly porous fcu-MOF (Metal-organic framework) chemi-capacitive sensor to detect H_2S gas at room temperature. That sensor was able to detect as low as 100 ppb H_2S and maintained good stability for 12 weeks. However, the sensor suffered from inadequate sensing response and high cross-sensitivity toward NO_2 gas.[33] In light of this drawback, there exists a need to improve the sensing performance by many folds to make it a suitable candidate for real-time sensing applications. In this regard, we propose an innovative sensor that includes a novel material and interdigitated electrode (IDE) based capacitive device (**Figure 1a (i)**) that can detect H_2S gas in trace amounts. In addition, the fabrication protocol of our sensor is compatible with the widely used Complementary metal-oxide-semiconductor (CMOS) process that enables large-scale production, substantially reducing the sensor cost. Our sensor is made up of four layers (Figure 1a), including Silicon (Si) substrate (ii), thermally grown 2 µm thick Silicon dioxide (SiO_2) (iii), interdigitated electrodes (IDE) (iv) and organic tris(keto-hydrazone) gas absorbent layer (v). A detailed explanation about the fabrication process of IDE sensor can be found under "sensor fabrication" heading in the experimental section. Followed by, the device image and the IDE device dimension details can be seen in Figure S1. The gas absorbent layer is specially made up of an HDN5 organic compound whose chemical structure can be seen in Figure 1b, belonging to tris(keto-hydrazone) family. Their unique behavior arises from their ability to tautomerization makes them a suitable material for various applications. As can be seen from the NMR data (Figure S2 and S3) the HDN5 material system undergo keto-imine

tautomerization, i.e. the hydrogen atom will be moving back and forth from nitrogen and oxygen giving rise to dynamism to the structure.

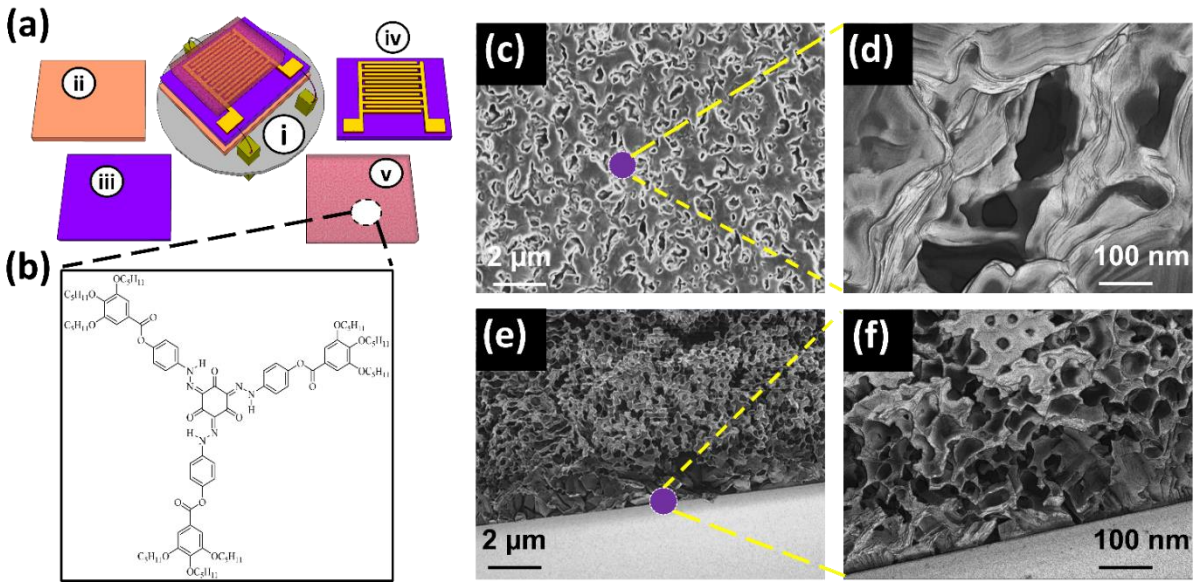

Figure 1. Sensor design: a) Top view of (i) interdigitated electrode (IDE) based capacitance sensor mounted on stand. The sensor is made up of (ii) Silicon substrate, (iii) Silicon oxide insulator layer, (iv) Ti / Au interdigitated electrodes on SiO_2 substrate and (v) gas receptor layer. b) Chemical structure of HDN5 organic compound. c) Low and d) High magnification surface FESEM images of the film. e) Low and f) High magnification cross-sectional FESEM images of the film on SiO_2/Si substrate.

To understand the nature and availability of porous structures, we have used FESEM technique to investigate the surface morphological properties of HDN5 film. From Figure 1c, uniform distribution of the pores with high density on the film surface of HDN5 can be witnessed. One of the pores was magnified to obtain details of its surface nature and cavity size. As can be seen in Figure 1d, multiple pores are found close to each other, whose sizes are around 100 nm. In addition, we have taken the cross sectional view of tris(keto-hydrazone) on Si/SiO_2 substrate to understand the distribution of pores on the sidewalls of the organic film (Figure 1e and f). Interestingly, pores can also be found on the sidewalls, whose pore sizes tend to be smaller than 100 nm, unlike the nature of pores on the surface. However, these dense

porous networks on the surface and sidewalls are highly beneficial in augmenting the surface area of the organic film that, in turn, improves the device sensing performance. A quick summary of the expected sensing mechanism from HDN5 film, when exposed to toxic gas molecules, is illustrated in **Figure 2a**. Keto hydrazones are explicitly selected considering the fact that they possess nitrogen-rich system which can act as a binding site for various acidic analytes such as H_2S. The tris(keto-hydrazone)s were prepared intentionally to increase the hydrazone binding sites i.e., compared to normal keto hydrazone tris(keto-hydrazone) has three hydrazones which can act as binding site for incoming analyste. The long alkaline chains were included to induce the behaviour of self-assembly and also to understand the steric effect on the detection of analytes. As can be seen in this figure, the dense porous structures enable the H_2S molecules to interact with gas-binding functional groups in the organic film.

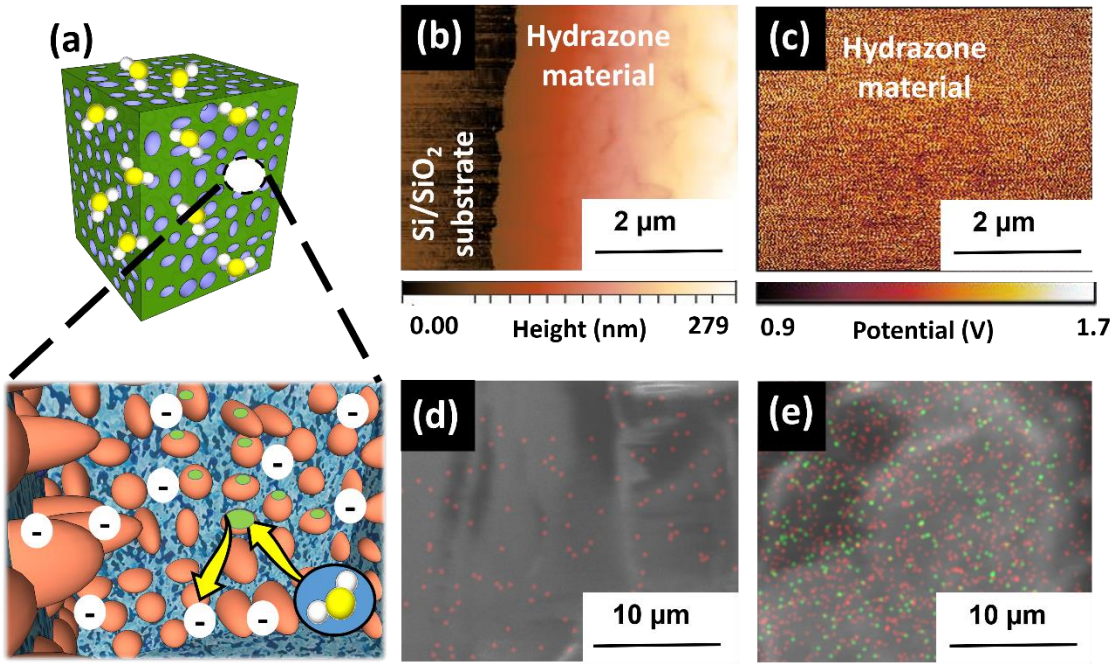

Figure 2. Material characterization of tris(keto-hydrazone) HDN5 organic film and sensing mechanism. a) The sensing mechanism of HDN5 material toward toxic gases. b) Film thickness and surface roughness measurement using AFM system and c) Contact potential difference (CPD) measurement using the KPFM characterization technique. EDX spectrum analysis of d) bare and e) H_2S exposed HDN5 film.

Using the Atomic force microscopy (AFM) technique, the thickness of the organic film was measured around 250 nm with a mean roughness of ~22 nm, as witnessed in Figure 2b. This high roughness is mainly due to the presence of dense porous structures. The electronic property of the organic film was probed using Kelvin probe force microscopy (KPFM) technique, as can be seen in Figure 2c. Through KPFM scanning, the mean contact potential difference (CPD) was measured to be around 1.653 V. In addition to this, it is vital to understand the effect of target H_2S gas on the optical properties of HDN5 organic film. Hence, we have probed the HDN5 thin-film using both Photoluminescence (Figure S4) and UV-Vis absorption (Figure S5) spectroscopy instruments. The common trend observed in both Figure S4 and S5 in Supporting information, the emission and absorption intensity of H_2S exposed organic sample decreased. This outcome suggests the presence of strong interaction between the H_2S and tris(keto-hydrazone), which is also a reversible reaction. To confirm this and to gain insights about the elements involved in the interaction, the EDX spectrum and the corresponding elemental analysis of the H_2S exposed sample was recorded. The Figure 2 (d & e) results confirmed that, after introducing H_2S gas, the Sulfur (S) elements from H_2S gas strongly interacts with the N_2 (N) elements of secondary amine group embedded in HDN5 tris(keto-hydrazone) framework. It is important to note that the observed properties are highly beneficial for achieving good sensing performance.

To reveal the sensing performance, primarily, the capacitance of an as-fabricated sensor was probed using LCR meter by applying an AC voltage of around 0.5 V at 100 kHz frequency. After probing 20 such sensors, we can witness that its average capacitance with standard deviation is around 193.4 ± 1.5 pF. This minimal deviation from the average capacitance shows that our device is reliable and the corresponding fabrication protocol is reproducible; hence the sensors are ready to be tested toward different gases to understand their gas sensing characteristics. Therefore, we have exposed the sensor to different concentrations of H_2S gas from 25 ppb to 25 ppm to probe its sensitivity (**Figure 3a**). Interestingly, our sensor was able

to detect as low as 25 ppb concentration in real-time conditions. The graph illustrating the non-linear gas response of our hydrazone capacitor sensor towards different H_2S gas concentration is presented in the Figure S6. Besides sensitivity, specificity is one of the crucial parameters to understand the figure of merit in the performance of a sensor. Therefore, we have tested our HDN5 device toward different toxic gases (each 25 ppm) and volatile organic compounds (VOCs) (each 1%). The transient response of our HDN5 sensor toward the tested analytes can be seen in Figure S76and S8 in supporting information.

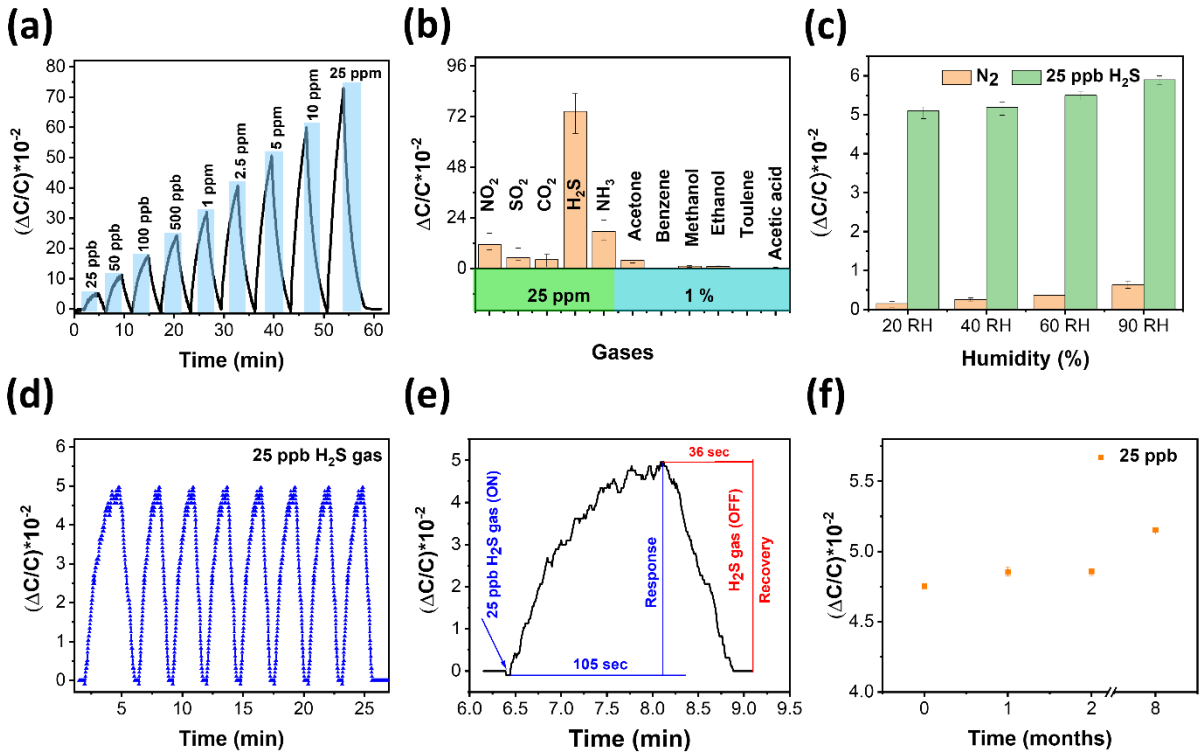

Figure 3. Gas sensing performance and stability of HDN5 capacitance sensor device. a) Transient response of IDE capacitor sensor towards different concentrations of H_2S gas from 25 ppb to 25 ppm ((Temperature condition : 22-23 °C) & Humidity (near to zero %RH – same as N2 (carrier gas) purge humidity)). b) Specificity of capacitance device toward oxidizing gases (25 ppm), reducing gases (25 ppm) and volatile organic compounds (1 % or 10,000 ppm) ((Temperature condition : 22-23 °C) & Humidity (near to zero %RH – same as N2 (carrier gas) purge humidity)). c) The effect of humidity (% RH) on the response of our sensor recorded during exposure to N_2 and (25 ppb) H_2S exposure (Temperature is 22-23 °C). d) Sensor repeatability study ((Temperature condition : 22-23 °C) & Humidity (near to zero %RH – same as N2 (carrier gas) purge humidity)) and e) Response and Recovery time of HDN5 tris(keto-hydrazone) sensor toward 25 ppb H_2S gas ((Temperature condition : 22-23 °C) & Humidity (near to zero %RH – same as N2 (carrier gas) purge humidity)). f) Ambient stability tested for 8 months in the presence of 25 ppb H_2S gas (Temperature (22-23 °C) and Humidity (40 %RH)).

As illustrated in Figure 3b, the HDN5 sensor exhibits exceptional specificity accompanied with good sensitivity ($\Delta C/C$) of around $72x10^{-2}$ toward 25 ppm H_2S gas. In addition, the device experiences a slight cross-sensitivity with NH_3 gas. Among all the tested VOC vapours, our HDN5 sensor exhibits good sensitivity toward acetone. However, its sensitivity is around 13.4 times smaller than the 25 ppm H_2S gas response. Hence, this study benchmarks the potential of our device in detecting the H_2S gas in the presence of other common interferrants. Moreover, it is 2 orders high in magnitude as compared to the work of Omar et al. .[33] In addition, we have compared our device sensing performance with the state of the art H_2S sensors reported in the literature since 2016, as shown in Table 1.

Table 1. Comparing our sensor performance with the reported H_2S sensors (since 2016)

Group	Sensing materials	Sensing mechanism	Sensitivity (ppm^{-1})	LOD (ppb)	Linear concentration (ppm)	Operating temperature	Stability studies
Metal oxides	ZnO nanowires [34]	Conductivity	20%	50	0.050 to 1	Room temperature (RT)	Not performed
Composite	ZIF-8 / ZnO nanorod [35]	Conductivity	5.21%	50	0.050 to 10	RT	Temperature effect (25 °C to 300 °C) and Effect of humidity (0 – 90% RH) Ambient stability (9 weeks)
2D materials	$MoSe_2$ nanoflakes [36]	Conductivity	10%	50	0.050 to 5	200 °C	Temperature effect (100 °C to 300 °C) and Ambient stability (1 month)
MOF	Ag_2O nano-decorated UiO-66 (Zr) BDC-NO_2 [37]	Chemi-capacitive	9%	1000	1 to 100	RT	Not performed
Organic	Ph5T2 [38]	Conductivity	100%	500	0.5 to 50	RT	Not performed
	Polypyrrole / WO_3 nanocomposite [39]	Conductivity	80%	100	0.1 to 1	RT	Effect of humidity (30% to 80% RH) and Ambient stability (55 days)
	Tris(keto-hydrazone) ***(current work)***	Chemicapactive	80%	25	0.025 to 25	RT	Temperature effect (20 °C to 100 °C), Humidity effect (20% to 95% RH), Bias stress (10 hours) and Ambient stability (50 days)

After that, the effect of relative humidity on the sensor response was investigated. Initially, moisture uptake by the organic film was studied by exposing the device toward water vapors having different humidity conditions from 20 to 90% RH. The transient response of the device towards different humidity conditions are showcased in Figure S9 in the supporting information. As can be seen in Figure 3c, under N_2 ambience, the response ($\Delta C/C$) of our sensor toward humidity varies from $0.2x10^{-2}$ @ 20% RH to $0.75x10^{-2}$ @ 90% RH. Whereas, after introducing 25 ppb H_2S gas in the testing gas chamber, the device response varies from $5.1x10^{-2}$ @ 20% RH to $5.8x10^{-2}$ @ 90% RH. This outcome shows that the effect of humidity is negligible on the sensing performance of our organic capacitor sensor. Furthermore, the response and recovery cycle was repeated eight times to demonstrate the reproducible performance of our sensor toward 25 ppb H_2S gas. As can be seen in Figure 3d, our sensor has shown exceptional repeatable nature having similar sensing response throughout tested cycles. It is important to note that our sensor can recover completely at room temperature avoiding the use of heat, light, or other forms of external energy source. In addition, our sensor takes around 105 sec and 36 sec to respond and recover toward 25 ppb H_2S gas, as witnessed in Figure 3e. Finally, the ambient stability of our capacitor sensor was tested in both presence and absence of target gases over a period of ~ 8 months. Before gas exposure, our sensor has shown exceptional stability with a small increase in the base capacitance around 3.8% from initial value after 8 months (Figure S10, Supporting information). Whereas, after introducing the target gas, a minimal fluctuation with just $0.5x10^{-2}$ ($\Delta C/C$) increase in sensor response is observed toward 25 ppb gas at the end of 8 months, as illustrated in Figure 3f. These results highlight the excellent ambient stability of our sensor.

The sensing mechanism behind the observed unprecedented performance is attributed to the presence of increased nitrogen concentration. It not only plays a key role in charge transfer and

enhancing the electrical properties of these compounds, but also these nitrogen atoms and imine groups act as binding sites for different small organic and inorganic compounds such as VOCs, metal ions, etc., which can be readily detected. These bulky systems, which are disc-shaped, tend to orient in the form of a column using thermal energy and undergo self-assembly structurally. This thermally driven self-assembly into the formation of columns is confirmed with the help of differential scanning calorimetry and polarizing optical microscopy (POM) studies. As can be seen from Table S1, these systems form the columnar liquid crystal phase around 80 °C. Figure S11 shows HDN-5 has a dipole moment of 0.77D. The electrostatic interaction of individual H_2S molecule with the HDN-5 molecule was studied and the subsequent dipole moment was determined. Upon addition of H_2S molecules, the dipole moment sharply increases by about 6 times in magnitude that leads to an increase in the relative permittivity, thereby increasing the capacitance. Similarly, it can be seen here that the higher steric energy (285.1 Kcal/mol) is observed in HDN-5, indicating a stronger steric interaction, which is also apparent from the data obtained after the addition of H_2S (Table S2). Using these data, it can be concluded that the selectivity of the HDN-5 towards H_2S detection can be attributed to both electronic as well as steric interactions.

The porous structures of the organic film resemble the dense cavities found inside the plant leaf structure. It is also observed that as there is a change in the tail length, the H_2S sensing ability also varied, indicating a strong correlation between the tail length driven self-assembly and the sensing ability of the compound (Table S2). Also, according to the acid-base reaction phenomenon, strong interaction can result in the release of charges in the form of HS^- ions. These excess charges, generated due to H_2S absorption, enables a strong displacement field inside the organic film when the external electric field is applied. The resultant displacement field will change the permittivity hence the dielectric constant of the material. The capacitance of the material is directly proportional to its dielectric constant. This cumulative effect is why our sensor displayed an excellent capacitance sensing response upon H_2S gas exposure.

Furthermore, the temperature of the gas chamber was varied from 22 °C (Room temperature) to 100 °C, while the device was exposed to 25 ppb H_2S gas. The sensor responses toward 25 ppb H_2S gas at different temperatures are presented in **Figure 4**. From this figure,

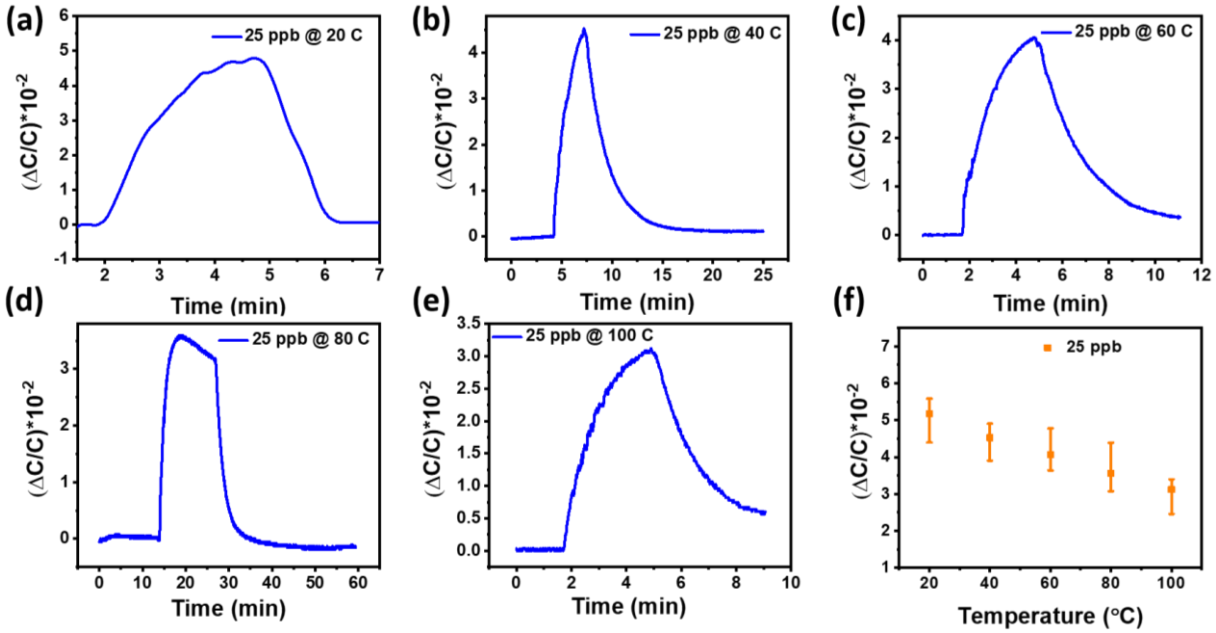

Figure 4. Transient response of capacitor device toward 25 ppb H_2S gas at a) 20 °C, b) 40 °C, c) 60 °C, d) 80 °C, e) 100 °C. f) Relation between the temperature and corresponding capacitance response of the sensor is plotted. The ambient condition: Humidity (near to zero %RH – same as N2 (carrier gas) purge humidity).

it is clear that the gas response nature was unaffected when the temperature was changed from 20 °C to 60 °C. Nevertheless, a significant decline in gas sensing response observed of around 60% when the temperature was varied from 60 °C to 100 °C. The thermal analysis carried out with the aid of polarizing optical microscopy (POM) and Differential scanning calorimetry (DSC) studies indicates the transition from crystal to liquid crystal behaviour at about 75 °C. As is well known, the crystal possesses the higher-order as compared with the liquid crystal phase. This loss of order with increasing temperature may be the root cause of a decrease in device response. The decrease in molecular order may lead to more fluctuations in the molecular level, which may alter the organic film's surface energy, leading to the substantial lowering of device response towards H_2S detection. The obtained results confirmed that our

HDN5 sensor has good air and moisture stability with good sensing response at room temperature.

3. Conclusion

To sum up, we have successfully demonstrated a room temperature operating novel solid-state HDN5 tris(keto-hydrazone) based chemi-capactive H_2S sensor. The sensor can detect a wide range of H_2S concentrations from 25 ppb to 25 ppm, having 25 ppb as an experimental limit of detection. When compared to the other tested toxic gases and VOCs, our sensor can specifically sense H_2S gas with high sensitivity. The stability study reveals that our organic capacitance sensor can maintain excellent sensing performance in the presence of continuous bias stress, humidity, and temperature (~60 °C). The unprecedented sensing characteristics of our sensor can strongly recommend the use of hydrazone based organic compounds as next-generation materials for sensing applications. Moreover, our sensor structure can yield multi-modal data provided we configure the measurement set-up.

4. Experimental Section

Synthesis of tris(keto-hydrazone): To synthesize tris(keto-hydrazone), initially, a well-stirred and cooled (-5 °C) solution comprising 4-aminophenyl 3,4,5-tris(pentyloxy)benzoate (0.48 mmol, 3 eq.) in 1:1 mixture of THF-methanol and 3 ml of a 2M HCl, a solution of $NaNO_2$ (0.02g, 0.32 mmol, 2 eq.) in 3 ml of water was added drop-wise slowly. The reaction mixture was allowed to warm up to room temperature to which a solution of phloroglucinol (0.02g, 0.159 mmol, 1 eq.) in methanol / 2M NaOH was added drop-wise. The reaction mixture was stirred for 30 mins. The pH of the reaction mixture was neutralized with dilute HCl, and the resultant mixture was poured into water and extracted with dichloromethane (3 × 30ml). The crude product was purified using column chromatography using neutral alumina. Initially, the column was eluted with hexanes, followed by 20% EtOAc-hexanes to obtain the desired

compound. This was further purified by recrystallization using absolute ethanol and corresponding details are given in supporting information

Surface characterization studies of tris(keto-hydrazone): Surface topography features of tris(keto-hydrazone) are explored using Field emission scanning electron microscopy (FESEM), Atomic force microscopy (AFM) and Kelvin probe force microscopy (KPFM). While using FESEM (Zeiss-Merlin) instrument, we have maintained Electron high tension (EHT) and safe working distance around 5.0 kV and 5.0 mm, respectively. In addition, high-resolution images of the material was captured with high-precision using the special In-Lens detector controlled by either analytical or high-resolution operating mode. We have used AFM Dimension-Icon (Veeco), operated in tapping mode, to probe the surface roughness and film thickness. During the AFM characterization experiment, we have optimized some of the crucial parameters like integral gain, proportional gain, amplitude set point and drive amplitude as 20.40, 4.294, 2.486 nm and 500 mV, respectively until the trace and retrace profiles are getting overlapped hence yielding high-quality surface AFM images. Finally, we have employed KPFM technique to obtain the surface potential map of tris(keto-hydrazone). Some of the settings such as integral gain, proportional gain, amplitude set-point, drive amplitude, lift scan height and input P-gain were optimized to 2.686, 5.00, 3.5 nm, 500 mV, 108.0 nm and 10.00 respectively. Thickness, surface roughness and contact potential difference (CPD) values were obtained by taking the average of the values that are measured from five different locations. The steps followed to extract mean CPD values from the KPFM map is provided below,

i. HOPG calibration step

The main purpose of this step is to find the work function of the tip (Φ_{tip}) using the standard highly oriented pyrolytic graphite (HOPG) sample.

$$\Phi_{tip} = e * (CPD) + \Phi_{HOPG} \quad (1)$$

It is well known that, the Φ_{HOPG} value is around 4.6 eV. By running AFM scans on the surface of HOPG sample using the standard AFM tip, we can able to obtain the relative domain potential maps wherein the mean CPD value is calculated. By feeding the mean CPD and Φ_{HOPG} values in the above equation (1), the Φ_{tip} was extracted, which is around 4.31 eV.

ii. Mean CPD value extraction

After HOPG calibration step, we have optimized some of the system parameters such as integral gain (20.40), proportional gain (4.294), amplitude set point (2.486), and drive amplitude (500 mV) before running both AFM and KPFM scans on the hydrazone sample. As a result, we obtain the scan data that is then processed using Gwyddion software. From this software, we can directly obtain the mean CPD values as reported in the manuscript.

Sensor fabrication: A n-type doped silicon wafer purchased from the industry (Si-mat) and used as a substrate to fabricate capacitor devices. Initially, the procured silicon wafers were sequentially cleaned in the cleanroom environment using the standard piranha recipe and buffer oxide etchant (buffered HF solution) to remove the native oxide layer. Without any further delay, the cleaned silicon wafers were loaded in the thermal growth system to grow a high-quality 2 µm SiO_2 layer via a wet oxidation approach on the surface of the Si substrate using a standard recipe. This was followed by the Si/SiO_2 wafer being ultrasonically cleaned in acetone and isopropanol (IPA) solvents for 5 min each before being rinsed in distilled (DI) water for a few minutes. We used a hotplate to heat the N_2 blown sample at 120 °C in an open environment for 5 min to remove the residual moisture. Using the standard photolithography process, the interdigitated electrodes were patterned on the surface of an Si/SiO_2 substrate. During this process, the substrate was uniformly coated with the widely used AZ-5214 positive photoresist using a spin coating technique. The photoresist-coated sample was heated at 110 °C for 2 min. Subsequently, the desired interdigitated electrode pattern was imaged on the surface of a photoresist-coated sample by exposing it to UV light (75 mJ dose for 7 sec) via a mask

containing the desired electrode design. The UV-exposed sample was developed in the AZ-726 developer. It is important to note that we carefully handled and processed the sample only in the yellow-light region during the photolithography process. After the development step, the sample was gradually taken into the white-light area to deposit the Titanium (Ti) and Gold (Au) metals at a thickness of around 10 nm and 100 nm, respectively, using a radio frequency (RF) sputtering instrument. The obtained sample was subjected to an ultra-sonication-guided lift-off process using acetone and IPA to realize the Ti/Au interdigitated source and drain electrodes, with a channel width (W) and length (L) of around 583,605 µm and 10 µm, respectively, on the surface of the Si/SiO_2 substrate. The source and drain deposited wafers were diced into individual substrates and used them to fabricate the gas sensors. The diced substrates were ultrasonically cleaned in acetone, IPA and water for 5 min each and then heated at 120 °C to remove the water residues. Followed by, the as-synthesized tris(keto-hydrazone) material was mixed with a chloroform solvent to prepare 5 mg/0.5 mL solution. We have taken 4 µL volume of the hydrazone solution and drop-casted on the surface of the interdigitated electrodes patterned on the surface of Si/SiO_2 substrate, and heated at 100 °C for 15 min to allow the complete evaporation of solvents; hence, we fabricated the hydrazone based capacitor devices. To achieve reproducible sensing characteristics, the same protocol was followed every time to fabricate capacitor sensor device.

Gas sensing experiments of chemi-capacitive sensor: We have installed a smart gas-set up to test the gas sensing performance of various devices. This set up consists of two mass flow controllers (MFCs) and one mass flow meter (MFM) whose operations are controlled by Personal computer (PC) via a LabVIEW program interface. The input side of the MFCs are connected to N_2 and testing gas cylinders whereas the output from the MFM block is connected to gas testing chamber. The chamber-lid is designed with a small holding feature attached on one side that helps us to plug and play the fabricated capacitor devices for testing purpose and

the electrical probes from LCR meter are connected to another side of the lid to monitor the device capacitance changes. The detailed explanation about the gas set up and its features can be found elsewhere.[19] Taking advantage of the two MFCs and N_2 inert diluting gas, we can precisely control the concentration of the toxic gases by maintaining an overall 200 SCCM gas volume flows into the chamber. To gain a better understanding of the standard conversion used to convert the desired gas concentration into the gas flow rate (sccm) via MFC, we have explained it below using an example,

For instance, we have purchased inorganic gases cylinders for testing the devices towards NO_2, SO_2, CO_2, H_2S, and Ammonia. During the gas sensing experiments, we have strictly maintained 200 sccm gas to flow into the chamber after diluting the toxic gases with the background nitrogen. The following formula is used to calculate the amount of gas exposed to the testing device.

Desired toxic gas concentration = (Desired toxic gas flow rate x toxic gas cylinder concentration) / (total gas permissible flow rate)

We know that, total permissible gas flow rate = 200 sccm.

In our experiments, we have used 1 ppm (toxic gas cylinder concentration) H_2S cylinder. Having this cylinder in place, with the help of the above equation, we need to dilute 5 sccm (desired toxic gas flow rate) of H_2S gas with 195 sccm of N_2 background gas to expose the device with 25 ppb (desired toxic gas concentration) gas whose 200 sccm flow rate is maintained while it is allowed to enter the cylinder.

Hence, we have rigorously followed the gas-flow control protocol during the gas sensing experiments.

As a result, using this sophisticated set-up, we have performed many gas sensing experiments to test the sensing behavior of tris(keto-hydrazone) sensor.

Stability studies related experiments: The stability of our organic capacitance sensor was tested against bias stress, relative humidity and ambient stability conditions. To study the effect of

bias stress effect on the sensing performance, the device under test was connected to the gas chamber and subjected to the fixed AC and DC voltage levels (as mentioned before) using LCR meter. During this study, the capacitance changes from the device before and after gas exposure was recorded every 2 hours. This study was conducted for a total period of 10 hours. For testing the device against humidity experiments, we have filled the DI water in the bubbler partially submerged in the temperature controller bath to maintain a constant temperature (in this experiment – 20 °C). By mixing the bubbler containing DI water with different volumes of N_2 gas, we were able to successfully control the relative humidity of gas chamber from 20% to 90% RH conditions. In addition, we were also able to pass the target toxic gas into the chamber without disturbing the relative humidity environment. These features enabled us to test the effect of different relative humidity conditions on the device response towards various gas concentrations. A long-term ambient stability experiment was conducted for the device's capacitance response toward the presence and absence of toxic gases. During this experiment, the device was stored in the normal laboratory conditions with neither special encapsulation nor a special environment used. The readings were taken for every 5 days extending over a total duration of 8 months and thereof. To test the reproducibility, instead of one device, we have followed the same protocols to record the results from four devices and the corresponding error bar data are plotted. This is followed for all the stability studies.

Supporting Information
Supporting Information is available from the Wiley Online Library or from the author.

Acknowledgements

This work was supported by the funding of King Abdullah University of Science and technology. Authors are thankful to the staff of the KAUST core labs, namely thin film (TF) lab, Nano-fabrication (NCL), and imaging and characterization (IAC) for their help throughout. CVY sincerely expresses his gratitude to SERB, Department of Science and Technology, Government of India.

Received: ((will be filled in by the editorial staff))
Revised: ((will be filled in by the editorial staff))
Published online: ((will be filled in by the editorial staff))

References

[1] a) H. Li, Y. Shi, G. Han, J. Liu, J. Zhang, C. Li, J. Liu, Y. Yi, T. Li, X. Gao, *Angewandte Chemie International Edition* **2020**, 59, 4380; b) B. M. Kilbride, M. Edmonds, J. Biggs, *Nature Communications* **2016**, 7, 1.

[2] C. Zhang, Y. Wang, S. Cheng, X. Zhang, B. Fu, W. Hu, *Advanced Electronic Materials* **2017**, 3, 1700209.

[3] a) T. Nguyen, T. Dinh, A. R. M. Foisal, H.-P. Phan, T.-K. Nguyen, N.-T. Nguyen, D. V. Dao, *Nature communications* **2019**, 10, 1; b) G. Konvalina, H. Haick, *Accounts of chemical research* **2014**, 47, 66.

[4] S. Yuvaraja, S. G. Surya, V. Chernikova, M. T. Vijjapu, O. Shekhah, P. M. Bhatt, S. Chandra, M. Eddaoudi, K. N. Salama, *ACS Applied Materials & Interfaces* **2020**, 12, 18748.

[5] Z. Sun, H. Yuan, Z. Liu, B. Han, X. Zhang, *Advanced Materials* **2005**, 17, 2993.

[6] Z. Li, N. Wang, Z. Lin, J. Wang, W. Liu, K. Sun, Y. Q. Fu, Z. Wang, *ACS applied materials & interfaces* **2016**, 8, 20962.

[7] W. Liang, J. Chen, L. Li, M. Li, X. Wei, B. Tan, Y. Shang, G. Fan, W. Wang, W. Liu, *ACS applied materials & interfaces* **2019**, 11, 14619.

[8] P. M. Bhatt, Y. Belmabkhout, A. H. Assen, Ł. J. Weseliński, H. Jiang, A. Cadiau, D.-X. Xue, M. Eddaoudi, *Chemical Engineering Journal* **2017**, 324, 392.

[9] J. H. Ko, Q. Xu, Y.-C. Jang, *Critical Reviews in Environmental Science and Technology* **2015**, 45, 2043.

[10] M. Gall, *Sensors and Actuators B: Chemical* **1993**, 16, 260.

[11] P. Krebs, A. Grisel, *Sensors and Actuators B: Chemical* **1993**, 13, 155.

[12] M. Jones, T. Nevell, *Sensors and Actuators* **1989**, 16, 215.

[13] S. Kolev, M. Ádám, C. Dücsö, I. Bársony, C. Cobianu, A. Van den Berg, *Microelectronics journal* **2000**, 31, 339.

[14] P. Zhao, Y. Zhao, H. Bao, H. L. Ho, W. Jin, S. Fan, S. Gao, Y. Wang, P. Wang, *Nature communications* **2020**, 11, 1.

[15] D. T. McQuade, A. E. Pullen, T. M. Swager, *Chemical Reviews* **2000**, 100, 2537.

[16] H. Omran, K. N. Salama, presented at 2015 IEEE 3rd International Conference on Smart Instrumentation, Measurement and Applications (ICSIMA) **2015**.

[17] D. Wong, O. Abuzalat, J. Ko, J. Lee, S. Kim, S. S. Park, *ACS Applied Materials & Interfaces* **2020**.

[18] S. Zhang, J. Wang, N. L. Torad, W. Xia, M. A. Aslam, Y. V. Kaneti, Z. Hou, Z. Ding, B. Da, A. Fatehmulla, *Small* **2020**, 16, 1901718.

[19] K. Govardhan, A. N. Grace, *Sensor Letters* **2016**, 14, 741.

[20] M. T. Vijjapu, S. G. Surya, S. Yuvaraja, X. Zhang, H. N. Alshareef, K. N. Salama, *Acs Sensors* **2020**.

[21] a) Y. Kumaresan, R. Lee, N. Lim, Y. Pak, H. Kim, W. Kim, G. Y. Jung, *Advanced Electronic Materials* **2018**, 4, 1800167; b) J. Leppäniemi, A. Sneck, Y. Kusaka, N. Fukuda, A. Alastalo, *Advanced Electronic Materials* **2019**, 5, 1900272.

[22] S. Yuvaraja, A. Nawaz, Q. Liu, D. Dubal, S. G. Surya, K. N. Salama, P. Sonar, *Chemical Society Reviews* **2020**, DOI: 10.1039/C9CS00811J.

[23] M. A. Andrés, M. T. Vijjapu, S. G. Surya, O. Shekhah, K. N. Salama, C. Serre, M. Eddaoudi, O. Roubeau, I. Gascón, *ACS Applied Materials & Interfaces* **2020**, 12, 4155.

[24] a) X. Liu, T. Fu, J. Ward, H. Gao, B. Yin, T. Woodard, D. R. Lovley, J. Yao, *Advanced Electronic Materials* **2020**, 2000721; b) J. Dai, H. Zhao, X. Lin, S. Liu, T.

Fei, T. Zhang, *Advanced Electronic Materials* **2020**, 6, 1900846; c) Z. Wang, Z. Liu, L. Chen, Y. Yang, J. Ma, X. Zhang, Y. Guo, G. Zhang, D. Zhang, *Advanced Electronic Materials* **2018**, 4, 1800025.
[25] X. Su, I. Aprahamian, *Chemical Society Reviews* **2014**, 43, 1963.
[26] R. Lazny, A. Nodzewska, *Chemical reviews* **2010**, 110, 1386.
[27] S. Kobayashi, Y. Mori, J. S. Fossey, M. M. Salter, *Chemical reviews* **2011**, 111, 2626.
[28] H. Y. Lee, X. Song, H. Park, M.-H. Baik, D. Lee, *Journal of the American Chemical Society* **2010**, 132, 12133.
[29] V. Chandrasekhar, R. Azhakar, B. Murugesapandian, T. Senapati, P. Bag, M. D. Pandey, S. K. Maurya, D. Goswami, *Inorganic chemistry* **2010**, 49, 4008.
[30] R. Riva, S. Schmeits, F. Stoffelbach, C. Jérôme, R. Jérôme, P. Lecomte, *Chemical communications* **2005**, 5334.
[31] J. Shao, Y. Qiao, H. Lin, H. Lin, *Spectrochimica Acta Part A: Molecular and Biomolecular Spectroscopy* **2009**, 71, 1736.
[32] V. Chernikova, O. Yassine, O. Shekhah, M. Eddaoudi, K. N. Salama, *Journal of Materials Chemistry A* **2018**, 6, 5550.
[33] O. Yassine, O. Shekhah, A. H. Assen, Y. Belmabkhout, K. N. Salama, M. Eddaoudi, *Angewandte Chemie International Edition* **2016**, 55, 15879.
[34] F. Huber, S. Riegert, M. Madel, K. Thonke, *Sensors and Actuators B: Chemical* **2017**, 239, 358.
[35] X. Wu, S. Xiong, Y. Gong, Y. Gong, W. Wu, Z. Mao, Q. Liu, S. Hu, X. Long, *Sensors and Actuators B: Chemical* **2019**, 292, 32.
[36] R. K. Jha, J. V. D'Costa, N. Sakhuja, N. Bhat, *Sensors and Actuators B: Chemical* **2019**, 297, 126687.
[37] S. G. Surya, S. Bhanoth, S. M. Majhi, Y. D. More, V. M. Teja, K. N. Chappanda, *CrystEngComm* **2019**, 21, 7303.
[38] X. Zhao, Y. Tong, Q. Tang, H. Tian, Y. Liu, *Organic Electronics* **2016**, 32, 94.
[39] P.-G. Su, Y.-T. Peng, *Sensors and Actuators B: Chemical* **2014**, 193, 637.

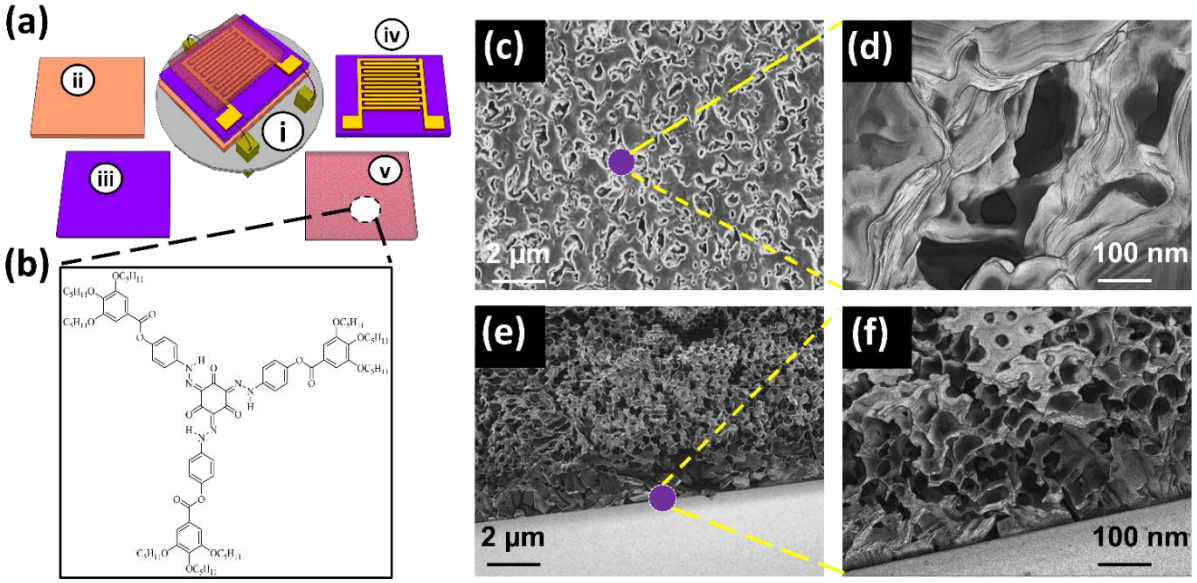

Figure 1. Sensor design: a) Top view of (i) interdigitated electrode (IDE) based capacitance sensor mounted on stand. The sensor is made up of (ii) Silicon substrate, (iii) Silicon oxide insulator layer, (iv) Ti / Au interdigitated electrodes on SiO_2 substrate and (v) gas receptor layer. b) Chemical structure of HDN5 organic compound. c) Low and d) High magnification surface FESEM images of the film. e) Low and f) High magnification cross-sectional FESEM images of the film on SiO_2/Si substrate.

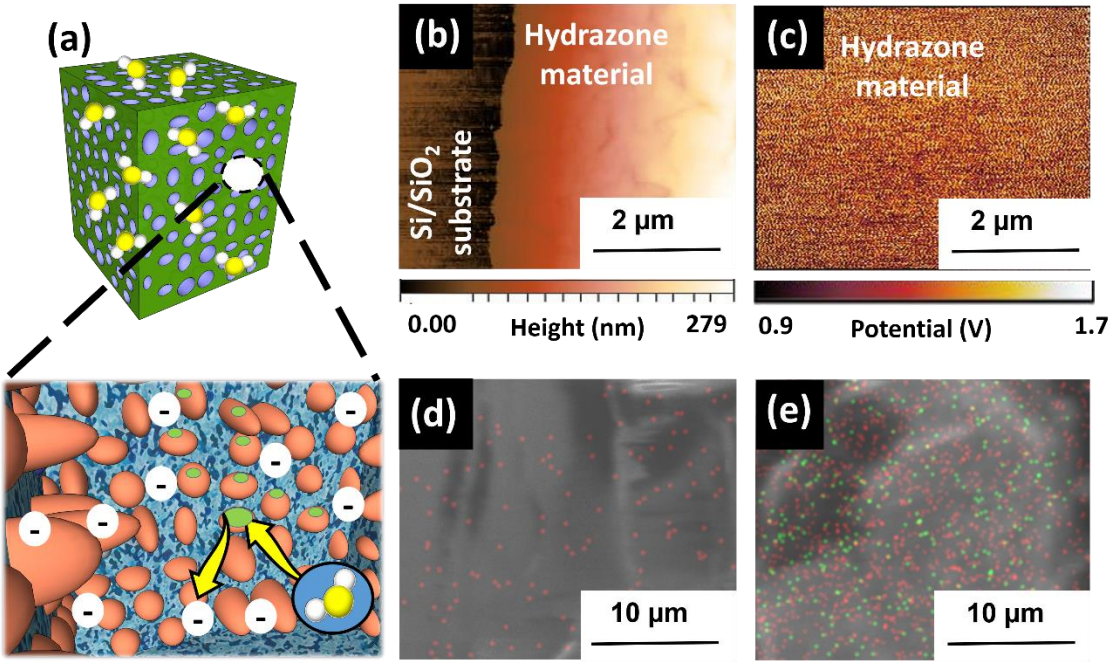

Figure 2. Material characterization of tris(keto-hydrazone) HDN5 organic film and sensing mechanism. a) The sensing mechanism of HDN5 material toward toxic gases. b) Film thickness and surface roughness measurement using AFM system and c) Contact potential difference (CPD) measurement using the KPFM characterization technique. EDX spectrum analysis of d) bare and e) H_2S exposed HDN5 film.

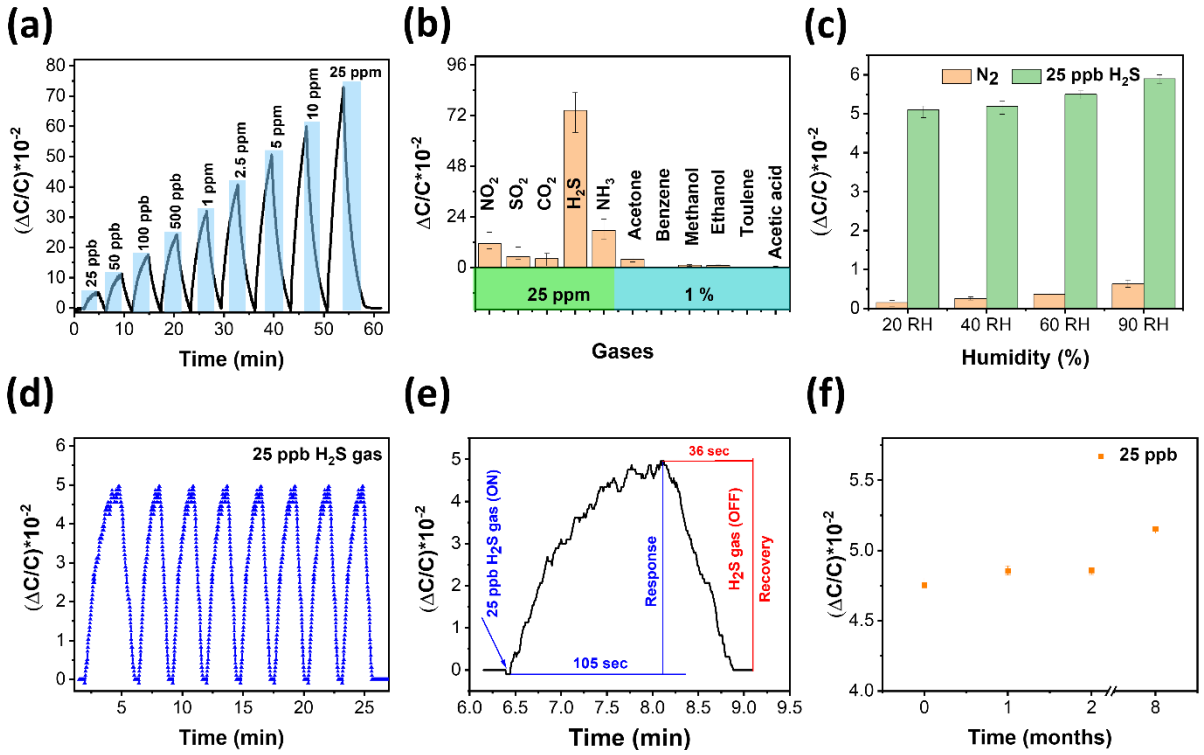

Figure 3. Gas sensing performance and stability of HDN5 capacitance sensor device. a) Transient response of IDE capacitor sensor towards different concentrations of H_2S gas from 25 ppb to 25 ppm ((Temperature condition : 22-23 °C) & Humidity (near to zero %RH – same as N2 (carrier gas) purge humidity)). b) Specificity of capacitance device toward oxidizing gases (25 ppm), reducing gases (25 ppm) and volatile organic compounds (1 % or 10,000 ppm) ((Temperature condition : 22-23 °C) & Humidity (near to zero %RH – same as N2 (carrier gas) purge humidity)). c) The effect of humidity (% RH) on the response of our sensor recorded during exposure to N_2 and (25 ppb) H_2S exposure (Temperature is 22-23 °C). d) Sensor repeatability study ((Temperature condition : 22-23 °C) & Humidity (near to zero %RH – same as N2 (carrier gas) purge humidity)) and e) Response and Recovery time of HDN5 tris(keto-hydrazone) sensor toward 25 ppb H_2S gas ((Temperature condition : 22-23 °C) & Humidity (near to zero %RH – same as N2 (carrier gas) purge humidity)). f) Ambient stability tested for 8 months in the presence of 25 ppb H_2S gas (Temperature (22-23 °C) and Humidity (40 %RH)).

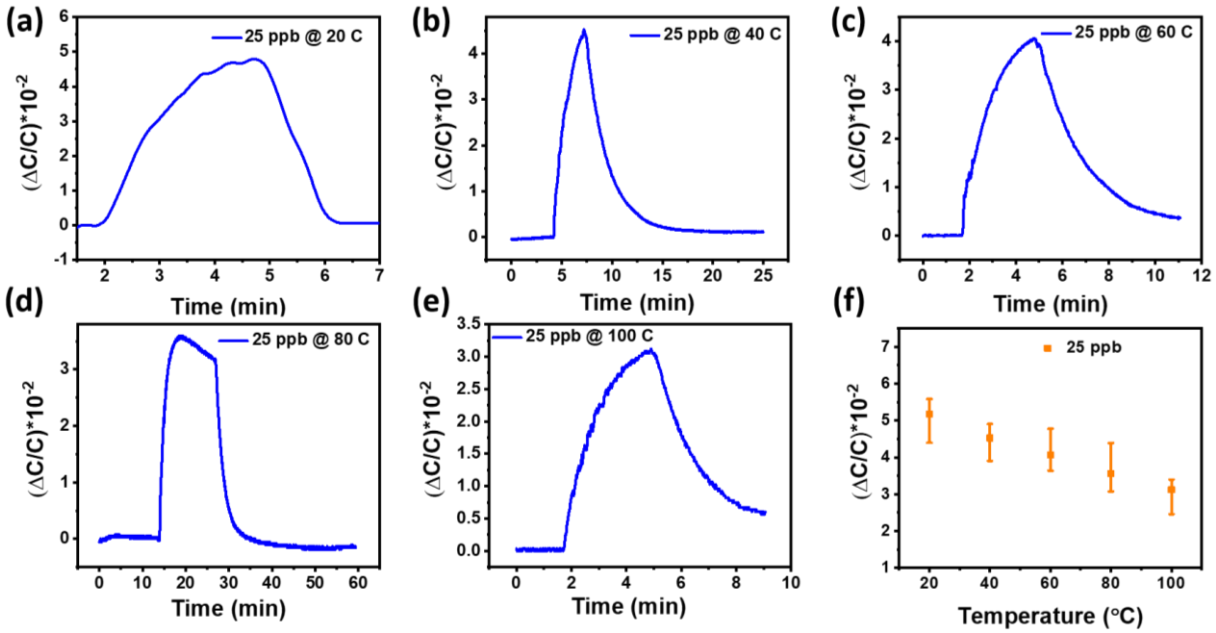

Figure 4. Transient response of capacitor device toward 25 ppb H_2S gas at a) 20 °C, b) 40 °C, c) 60 °C, d) 80 °C, e) 100 °C. f) Relation between the temperature and corresponding capacitance response of the sensor is plotted. The ambient condition: Humidity (near to zero %RH – same as N2 (carrier gas) purge humidity).

Table 1. Comparing our sensor performance with the reported H_2S sensors (since 2016)

Group	Sensing materials	Sensing mechanism	Sensitivity (ppm^{-1})	LOD (ppb)	Linear concentration (ppm)	Operating temperature	Stability studies
Metal oxides	ZnO nanowires [34]	Conductivity	20%	50	0.050 to 1	Room temperature (RT)	Not performed
Composite	ZIF-8 / ZnO nanorod [35]	Conductivity	5.21%	50	0.050 to 10	RT	Temperature effect (25 °C to 300 °C) and Effect of humidity (0 – 90% RH) Ambient stability (9 weeks)
2D materials	$MoSe_2$ nanoflakes [36]	Conductivity	10%	50	0.050 to 5	200 °C	Temperature effect (100 °C to 300 °C) and Ambient stability (1 month)
MOF	Ag_2O nano-decorated UiO-66 (Zr) BDC-NO_2 [37]	Chemi-capacitive	9%	1000	1 to 100	RT	Not performed
Organic	Ph5T2 [38]	Conductivity	100%	500	0.5 to 50	RT	Not performed
	Polypyrrole / WO_3 nanocomposite [39]	Conductivity	80%	100	0.1 to 1	RT	Effect of humidity (30% to 80% RH) and Ambient stability (55 days)
	Tris(keto-hydrazone) ***(current work)***	Chemicapactive	80%	25	0.025 to 25	RT	Temperature effect (20 °C to 100 °C), Humidity effect (20% to 95% RH), Bias stress (10 hours) and Ambient stability (50 days)

The work demonstrates a capacitive sensor based on Tris(keto-hydrazone) monomer that detects H_2S gas with ultra-sensitivity. Such a system consists of a porous monomer that can readily absorb and react with toxic gases, eventually changing the capacitance of the device. The proposed sensor is a highly stable, specific , scalable, and easy process tool that can help in taking preventive measures.

Saravanan Yuvaraja[1‡],Veerabhadraswamy N. Bhyranalyar[2‡], Sachin A. Bhat[2], Mani Teja Vijjapu[1], Sandeep G. Surya[1], C. V. Yelamaggad[2]*, and Khaled Nabil Salama[1]**

Title: Tris(Keto-Hydrazone): A fully integrated highly stable and exceptionally sensitive H_2S capacitive sensor